Wideband transmitarrays based on anisotropic unit-cells for next generation sub-THz applications

Orestis Koutsos, Francesco Foglia Manzillo, Antonio Clemente, Ronan Sauleau

Wideband Transmitarrays based on Anisotropic Unit-Cells for Next Generation sub-THz Applications

Orestis Koutsos[1,2], Francesco Foglia Manzillo[1], Antonio Clemente[1], Ronan Sauleau[2]
[1] CEA-Leti, Univ. Grenoble-Alpes, F-38054 Grenoble, France ({francesco.fogliamanzillo, antonio.clemente}@cea.fr)
[2] Univ Rennes, CNRS, IETR – UMR 6164, F-35000 Rennes, France ({orestis.koutsos, ronan.sauleau}@univ-rennes1.fr)

***Abstract*—This paper presents an anisotropic transmitarray for next-generation applications in the 300-GHz band. First, the proposed three-layer unit-cell is analyzed theoretically to demonstrate its effectiveness in transmission and bandwidth operation. Then, two designs using different manufacturing technologies are synthesized. The first one is based on a standard printed circuit board process to represent a low-cost solution. The second one uses lithography in fused quartz, leveraging a higher fabrication and transmission phase resolutions for more efficient transmitarray design. Based on the two structures, two 40×40-element prototypes are realized considering these two fabrication streams. The low-cost prototype is measured, achieving a peak gain of 32.2 dBi with 31.8% aperture efficiency and a 3-dB gain bandwidth of 55 GHz (19%).**

***Index Terms*—Transmitarray, anisotropy, sub-THz, printed circuit board, quartz lithography.**

I. Introduction

The sub-THz band of the millimeter-wave (mm-wave) spectrum holds great potential in offering high resolution and large absolute bandwidth. These features are essential for next-generation applications including imaging processes and high-speed communications. In all wireless sub-THz systems, high-gain and wideband antennas are required to mitigate the high propagation losses and exploit efficiently the available bandwidth. To this end, spatially-fed architectures are the most common candidates, since they do not employ feed networks, as in the case of standard phased arrays [1]. Dielectric lenses are often preferred, thanks to their excellent radiation performance. However, their pattern optimization is based on adjusting the lens shape ([2] – [4]) or using multiple shells, e.g. Fly's Eye lenses [5], leading to increased material losses and bulkier configurations.

Transmitarrays (TAs) inherit the advantages of lenses, allowing for a flexible and more efficient pattern synthesis [6], while keeping a compact profile. In addition, in contrast to reflectarray antennas, they do not suffer from feed blockage; moreover, they are compatible with planar manufacturing processes, including low-cost techniques, such as standard printed circuit board (PCB). Nonetheless, the choice of fabrication stream and the maximum achievable performance depend on the selection of the periodic unit-cell (UC), focusing always on the optimization of three parameters; the magnitude, the phase and the bandwidth of transmission. There are already a few prototypes realized in PCB that can be found up to D-band. The selected UCs are based either on

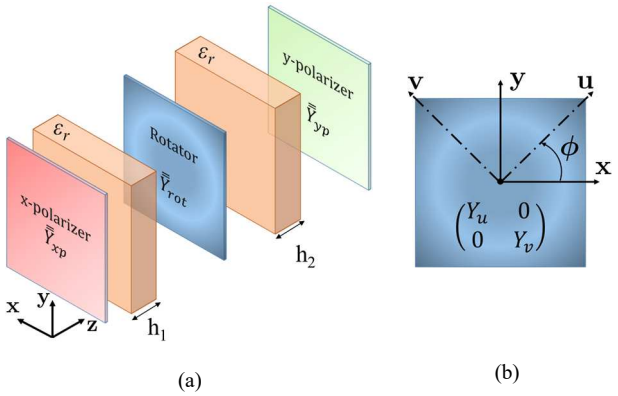

Fig. 1. (a) Exploded view of the anisotropic unit-cell. Each metal layer is illustrated by a different colors to highlight the anisotropic behavior. Two dielectric spacers, depicted in orange color, are placed in between to hold the structure all-together. (b) Diagram of an arbitrary rotator layer with its admittance matrix that describes its properties in the crystal system (u,v) and is used in the reference system (x,y) of the UC.

antenna-filter-antenna (AFA) topologies [7] or on frequency-selective surfaces (FSS) [8] by stacking multiple layers. However, once reaching the upper-end of the mm-waves, around 300 GHz, the proposed structures cannot overcome the technological constraints of the PCB, as in [7], or they exhibit narrowband operation, as in [8]. Therefore, the main approach has been to consider more advanced technologies, such as low temperature co-fired ceramic (LTCC), as presented at D-band in [9]. To avoid such solutions, an alternative UC comprising three asymmetric layers for anisotropic transmission can be found [10]. In theory, the structure can target efficiently all three parameters of transmission. Furthermore, by varying only the geometry of the inner layer, it is possible to tune completely the phase of transmission with small reflection losses, making this topology attractive for TA applications.

We report here two different designs of the anisotropic UC, targeting wireless applications in the unexploited region between 250 – 325 GHz. Each design is based on a different fabrication process, in order to present a low-cost solution and demonstrate the efficient performance of the proposed TA antennas. The analysis of the UC presented in Section II is based on a theoretical model reported in [11]. Finally, two low-profile prototypes are realized, exhibiting high aperture efficiency and wideband operation. A gain comparison of the two antennas is given to demonstrate the potential of this

anisotropic TA in achieving near-optimal operation, close to that of an ideal TA.

II. Unit-Cell Analysis

The proposed UC is represented in Fig. 1(a). The stacked configuration comprises three asymmetric metal layers, which are held together using two substrates. Each layer is used for a different polarization state, so that the UC can achieve maximum transmission and polarization conversion at the same time. This property is described theoretically by the transmission coefficient T_{yx} or T_{xy} for each side of propagation, respectively. The outer layers are used as polarizers for orthogonal polarization states in the (x,y) system. Moreover, the middle layer, named rotator, is responsible for coupling the x- and y-polarizations, which is an essential part for tuning the phase of transmission T_{yx}.

To facilitate the design process while targeting the maximum performance, a numerical model based on the transfer-matrix approach cascading admittance sheets is employed. Each layer is modelled by a 2×2 admittance matrix to take into account the asymmetries on all layers. This matrix is diagonal for both polarizers (external metal layers) and non-diagonal for the rotator, assuming a mode coupling through the admittance factors Y_{yx} and Y_{xy}. To avoid the coupling factors, which are generally hard to control, the matrix of the rotator is diagonalized. Specifically, by applying a rotation transformation between the UC reference system (x,y) and the rotator crystal system (u,v) by an angle ϕ, a new diagonal admittance matrix can be used, as shown in Fig. 1(b). The two new values of admittance, namely Y_u and Y_v, are used in the numerical analysis and the TA design, as reported in [11]. Finally, the two dielectric spacers are expressed by a standard transmission line model, using their thicknesses and permittivity in the calculation of the wave impedance inside the corresponding medium.

The key element for the efficient TA design is the rotator. Moreover, the selection of the spacers is also very important for targeting the maximum performance. Specifically, when the spacers are identical, a locus for perfect transmission and complete phase coverage (360°) can be found. This locus is depicted by a dark solid curve in Fig. 2(b). In this case, the thicknesses of the spacers are set to $h_1 = h_2 = 0.25\lambda$, λ being the wavelength inside the dielectric. In this case, all materials are assumed lossless. However, if the spacers are not identical, then no solution for perfect transmission with complete phase coverage can be found unless including larger reflection losses in the TA. For example, in Fig. 2(a), when the thicknesses are set to $h_1 = 0.25\lambda$ and $h_2 = 0.125\lambda$, the phase coverage is less than 190°, assuming 1 dB of maximum reflection losses. In order to take into account the rest of the corresponding phase, 3 dB of maximum reflection losses must be considered. Based on this model, it can be found that the larger the difference of the two thicknesses is, the worse become the reflection losses targeting complete phase coverage. Finally, based on the solutions given in Fig 2(b), the rotator must exhibit unrealistic behavior, targeting complete transmissivity ($Y_u = 0$) and complete reflectivity ($Y_v \rightarrow -\infty$), respectively, or vice versa.

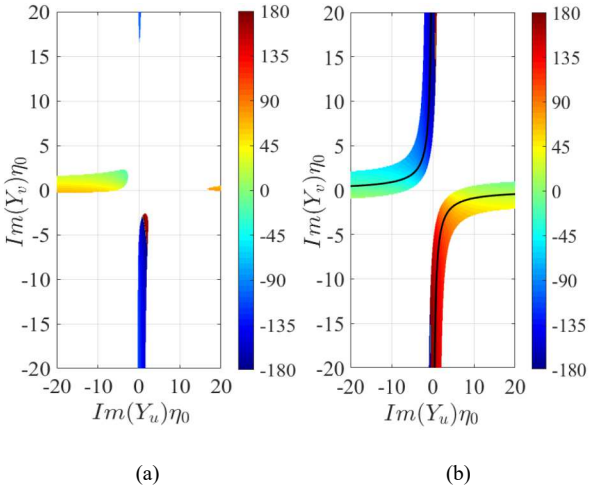

Fig. 2. Phase of transmission, T_{yx}, as a function of the rotator normalized admittance that describes its properties in the crystal system (uv). The polarizers are assumed ideal; the spacers have a permittivity $\varepsilon_r = 3$ and thicknesses equal to (a) $h_1 = 0.25\lambda$, $h_2 = 0.125\lambda$ and (b) $h_1 = h_2 = 0.25\lambda$. Both graphs depict only the part of the phase where the reflection loss is less than 1 dB. The solid curve in (b) represents the solutions of the admittance pairs (Y_u,Y_v) where there is perfect transmission.

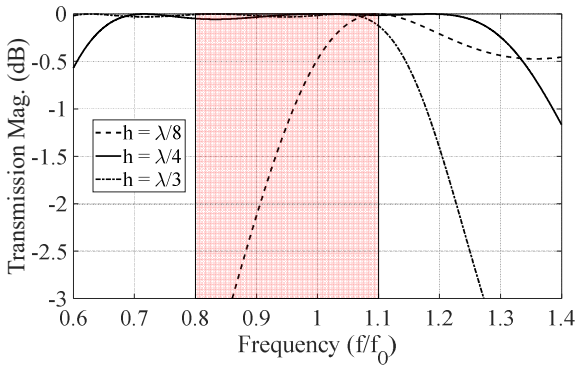

Fig. 3. Magnitude of transmission T_{yx} of the unit-cell as a function of normalized frequency for different spacer thicknesses, assuming that they are identical ($h_1 = h_2 = h$). The colored area represents the equivalent bandwidth 240 – 330 GHz, considering a cental frequency of 300 GHz.

The next step is to assess the bandwidth performance of the structure, which is very important for the TAs. Once again, a theoretical limit can be defined by studying the spacers, which are now assumed identical for the reasons explained before. As shown in Fig. 3, the UC can cover almost 100% relative bandwidth with near-zero reflection losses, when both spacers exhibit quarter-wavelength thicknesses. Nevertheless, even when such a thickness size is not commercially available, the structure can still be relatively wideband, targeting an operation around the central frequency. For instance, for a thickness equal to λ/3, the (normalized) frequency region between 0.8 – 1.1 is fully covered with almost no reflection losses, as shown in Fig. 2. This is important for practical reasons because, in planar fabrication processes, e.g. PCB, it is difficult to find the exact desired value of thickness, especially in sub-THz frequencies.

Finally, in the previous study, the polarizers are assumed ideal for simplicity. In case of using actual topologies, two

strip gratings with orthogonal orientations can be used for the description of their admittance matrix. Their properties have been thoroughly studied previously, as in [12], showing good performance for both reflectivity and transmissivity. In this scenario, some minor reflection losses will be added in the final transmission. If both gratings are designed correctly, the corresponding reflection losses will be kept less than 0.5 dB around the central frequency.

III. Unit-Cell Design

To demonstrate the effectiveness of the anisotropic UC in transmission and low-cost solution, two designs are proposed. The first one takes into account very strict fabrication constraints, considering standard industrial design rules for PCB fabrication, targeting a minimum of 3-bit phase resolution on the TA in order to minimize the quantization loss. The second UC is based on fused quartz substrates (patterned by photolithography), leading to a better phase resolution and improved performance of the antenna system. Both proposed designs are optimized for TA applications in the region 250 – 325 GHz.

A. Unit-Cell design in PCB

The UC in PCB is shown in Fig. 4(a). Two low-loss Isola Astra MT77 substrates and a bonding layer with low permittivity (ε_r = 3) are used. To target the maximum theoretical bandwidth around the center frequency, the thicknesses are set to h_1 = 127 µm and $h_2 = h_g$ = 64 µm, which are the closest values to a quarter-wavelength spacing between the layers, provided by the manufacturer. In addition, a minimum resolution of 80 µm in the conductor width and spacing is considered in the design process. To avoid the onset of higher-order diffraction modes in the bandwidth of interest, the periodic size of the UC is set to P = 500 µm ($\lambda_0/2$ at 300 GHz). Specifically, with this lattice size, the first onset of higher-order modes occurs around 350 GHz ($1.17\lambda_0$ w.r.t. 300 GHz) in free space, assuming 45° of maximum angle of illumination. This allows for safe TA designs with a focal-to-diameter (F/D) ratio down to 0.5.

Due to the strict specifications of standard PCB design rules and fabrication constraints, different geometries of the rotator were employed. A simple straight dipole was selected as the initial geometry and it was used as a reference. This shape is derived immediately by observing the admittance pairs Y_u and Y_v that give a solution of perfect transmission, as showed in Fig. 2(a). Specifically, the rotator must exhibit purely capacitive and inductive properties for each polarization, respectively, along the crystal axes. Then, by incorporating additional metallic parts on the straight dipole, different shapes were constructed, as shown in Fig. 4(b). This allows tuning the transmission phase with more flexibility, while focusing on the admittance pairs giving perfect transmission. Four shapes were found (UC1 to UC4), enabling a 3-bit TA design, since the 4 remaining shapes are derived by mirroring the rotator with respect to the x- or y-axis. In the case of the polarizers, the width and spacing of the two strip gratings are set to 80 µm and 170 µm, respectively. This leads

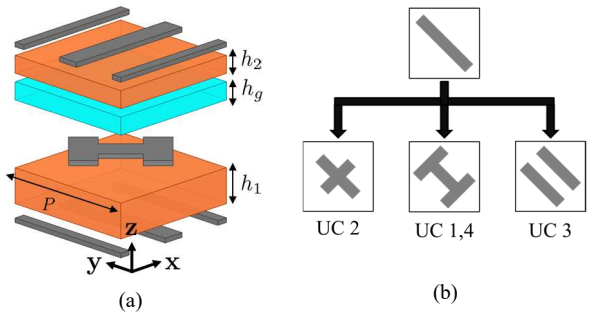

Fig. 4. (a) 3D exploded view of the UC realized in PCB. (b) Design approach of the rotator layer. Starting from a simple dipole, different shapes are defined, targeting each time a desired admittance pair in the crystal axes, as described in Section II.

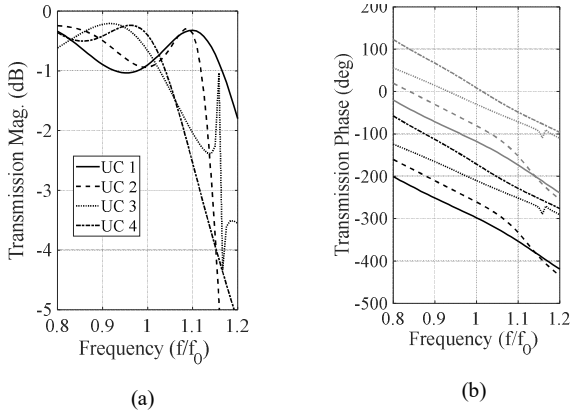

Fig. 5. Simulated T_{yx} in magnitude (a) and phase (b) of the PCB unit-cells. The phase of transmission for the mirrored cases is depicted in gray color. The central frequency, f_0, is equal to 300 GHz.

to a filling factor equal to 0.32, resulting in 0.25 dB of minimum reflection loss, calculated theoretically.

Fig. 5 shows the simulated results of the magnitude and phase in transmission of the final designs. Each UC covers at least an 80-GHz bandwidth with less than 1 dB of reflection loss. The upper 1-dB band edge goes up to 315 GHz ($1.05f_0$) and is extended down to almost 200 GHz ($0.67f_0$). The maximum frequency where all UC remain operational is about 330 GHz ($1.1f_0$). Finally, the absolute relative phase error between adjacent states is kept less than 20° around the central frequency, but it becomes worse for frequencies larger than 330 GHz ($1.1f_0$).

B. Unit-Cell design in quartz lithography

The second proposed configuration is shown in Fig. 6(a). The selected technology is based on photolithography process of quartz substrates. The precision in the metallic layers can reach a few µm. Nevertheless, to avoid fabrication errors, the minimum pattern resolution is set to 20 µm. Thanks to such

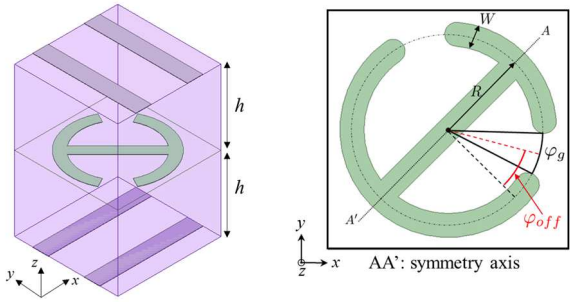

(a) (b)

Fig. 6. View of the UC using quartz substrates and (b) rotator geometry employed for the TA design. This UC exhibits a periodic size 2.5 times smaller than the PCB-based structure.

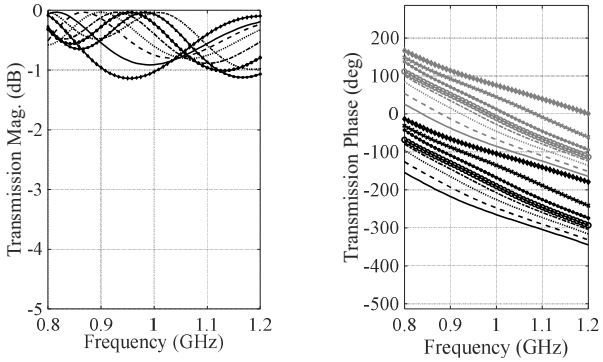

(a) (b)

Fig. 7. Magnitude (a) and phase (b) of T_{yx} for the designed quartz UC. The mirrored cases in the phase of transmission are depicted in grey color. All UC use the same rotator topology (Fig. 6b); the transmission phase is tuned by varying their angle φ_g from 20° to 50° and the angle φ_{off} from 0° to 40°.

accuracy, it is possible to target a subwavelength periodic size, equal to $P = 200$ µm ($\lambda_0/5$ at 300 GHz), making the structure more robust for larger angles of illumination, compared to the PCB unit-cells. The thickness of both quartz substrates is set to $h = 144$ µm, which is the closest value to a quarter-wavelength size that can be found commercially, given a permittivity equal to $\varepsilon_r = 3.78$.

The rotator is a combination of a dipole and a circular split ring with two identical cuts. The transmission in magnitude is optimized by fixing the dipole length $L = 2R$ at a center frequency. Then, the transmission phase is tuned by modifying the two arcs of the ring through the opening angle φ_g and the orientation angle φ_{off}, as shown in Fig. 6(b). Therefore, the design approach is similar as before, but using only one type of geometry. Finally, the width and spacing of both polarizers are set to 30 µm and 70 µm, respectively.

Based on this rotator, a 4-bit TA design is derived. The magnitude and phase of transmission are shown in Fig. 7. The results show an ultra-wideband operation, covering more than 50% of fractional bandwidth and improving the transmission at higher frequencies compared to the PCB design. Finally, the absolute phase error is kept less than 5° around the center

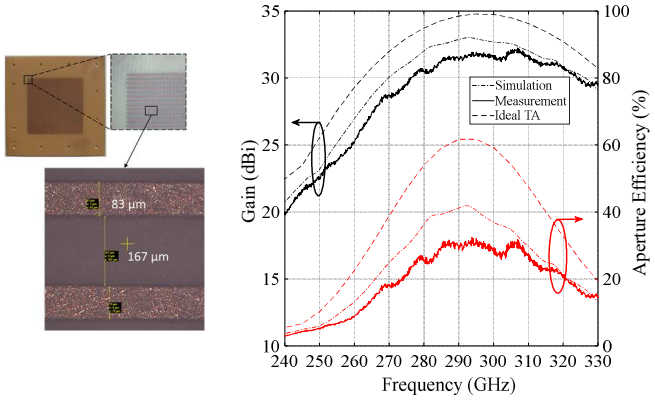

(a) (b)

Fig. 8. 3D exploded view of the UC realized in PCB. (b) View of the fabricated TA prototype, showing the dimensions of the strip grating. (c) Simulated and measured gain and aperture efficiency of the antenna prototype. The results are compared to an antenna comprising a perfect lens, considering the same focal source and focal distance.

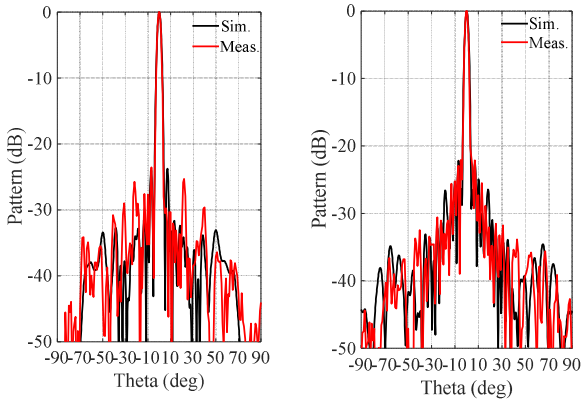

(a) (b)

Fig. 9. Simulated and measured radiation pattern of the TA at 290 GHz in (a) H-plane and (b) E-plane.

frequency and it becomes larger at higher frequencies since the UCs were not optimized for TA applications in this region. Based on these results, the quartz design is one of the most wideband configurations in sub-THz frequencies compared to the literature.

IV. Transmitarray Design

To examine and compare the radiation performance of the two proposed unit-cells, two TA prototypes are designed. In both cases, the size of the TA is set to 20×20 λ^2 at 300 GHz, targeting a peak gain of 35 dBi. This gives a 40×40-element and a 100×100-element TA for the PCB and the quartz design, respectively. Both arrays are illuminated using a standard pyramidal horn with 10 dBi nominal gain (model 32240-10 by Flann). Their phase distribution is calculated for maximum gain operation at 280 GHz, which is approximately the center frequency of the targeted frequency bandwidth. The

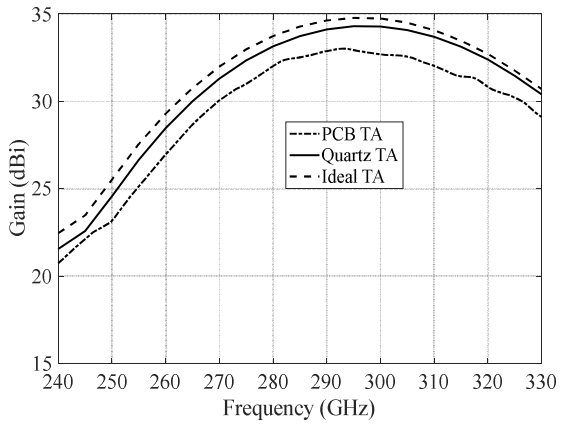

Fig. 10. Frequency responses of the PCB and quartz TA. Comparison with an ideal TA.

optimization of both TAs is based on a hybrid simulation tool using standard ray tracing techniques and far-field quantities. For both designs, the optimal focal distance is found to be 11 mm, corresponding to a ratio F/D = 0.55 and a low-profile system.

The PCB prototype was fabricated and experimentally characterized in the CEA-Leti far-field anechoic chamber. A picture of the prototype is shown in Fig. 8(a). The results in gain and aperture efficiency are plotted in Fig. 8(b) as a function of frequency. The maximum measured gain and the corresponding aperture efficiency are 32.2 dBi and 31.8%, respectively, at 307 GHz. The maximum aperture efficiency equals 32.4% at 293 GHz which is shifted by 5% with respect to the design frequency due to a small error (+0.5mm) in the focal distance. The 3-dB gain bandwidth is about 55 GHz (19%), from 272 to 330 GHz, covering most of the desired bandwidth. The aperture efficiency remains larger than 25% between 277 GHz and 312 GHz. The maximum gain loss is about 2 dB and 2.5 dB in simulation and measurement, respectively, compared to an ideal TA design with the same type of illumination. Finally, the half-power beamwidth is about 3° and is very stable in the 3 dB gain bandwidth. Two orthogonal cut planes of the radiation pattern are plotted in Fig. 9. The simulated and measured results of the patterns are in a good agreement and the maximum side lobe level is about – 23 dB and – 22 dB in the H- and E-plane, respectively.

Finally, the simulated peak gain response of the 4-bit quartz prototype, compared to the results of the PCB prototype and the ideal TA, is shown in Fig. 10. Using a finer fabrication accuracy, it becomes possible to target the optimal radiation performance in the TA antenna, with a gain loss lower than 0.5 dB if compared to the ideal transmitarray.

V. Conclusion

A low-cost and efficient TA design for next-generation applications at 300 GHz was presented. The three-layer anisotropic unit-cell can achieve near-perfect transmission in a very large bandwidth, which was demonstrated rigorously using a theoretical model. A PCB-based TA with 3-bit phase resolution was fabricated and measured. The antenna system exhibits a low-profile, attaining high radiation performance in a relatively large bandwidth. Finally, an improved TA design concept considering a quartz lithography for future fabrication was proposed. The new periodic element can improve the transmission in higher frequencies and achieve a higher phase resolution on the TA, paving the way for the realization of future artificial lenses with near-perfect performance.

Acknowledgment

This work was supported in part by the National Research Agency (ANR) through the project “Next5G” under Grant ANR 18-CEA 25-0009-01.

References

[1] S. Li, Z. Zhang and G. M. Rebeiz, "An eight-element 136–147 GHz wafer-scale phased-array transmitter with 32 dBm peak EIRP and >16 Gbps 16QAM and 64QAM operation," in *IEEE J. Solid-State Circuits*, vol. 57, no. 6, pp. 1635-1648, June 2022.

[2] B. Barès, R. Sauleau, L. Le Coq, and K. Mahdjoubi, "A new accurate design method for millimeter-wave homogeneous dielectric substrate lens antennas of arbitrary shape," in *IEEE Trans. Antennas Propag.*., vol. 53, no. 3, pp. 1069-1082, Mar.s 2005.

[3] R. Sauleau and B. Barès, "A complete procedure for the design and optimization of arbitrarily-shaped integrated lens antennas," in *IEEE Trans. Antennas Propag.*, vol. 54, no. 4, pp. 1122-1133, Apr. 2006.

[4] N.T. Nguyen, A.V. Boriskin, A. Rolland, L. Le Coq, and R. Sauleau, "Shaped lens-like dome for UWB antennas with a gaussian-like radiation pattern," in *IEEE Trans. Antennas Propag.*, vol. 61, no. 4, pp. 1658-1664, Apr. 2013.

[5] M. A. Campo *et al.*, "Fly's eye lenses for wideband beyond 5G communications," in *2020 45th International Conference on Infrared, Millimeter, and Terahertz Waves (IRMMW-THz)*, Buffalo, NY, USA, 2020, pp. 1-1.

[6] F. Foglia Manzillo, O. Koutsos, B. Fuchs, R. Sauleau and A. Clemente, "Synthesis and Characterization of a Focused-Beam Transmitarray Antenna at 300 GHz," in *2022 16th Eur. Conf. Antennas Propag. (EuCAP)*, Madrid, Spain, 2022, pp. 1-4

[7] F. Foglia Manzillo, A. Clemente and J. L. González-Jiménez, "High-gain D-band transmitarrays in standard PCB technology for beyond-5G communications," in *IEEE Trans. Antennas Propag.*, vol. 68, no. 1, pp. 587-592.

[8] D. Seo, H. Kim, S. Oh, J. Kim and J. Oh, "Ultra-thin high gain D-band transmitarray based on a spatial filter topology utilizing bonding layer effect," in *IEEE Antennas Wirel. Propag. Lett. (Early Access)*, 2022.

[9] Z. -W. Miao *et al.*, "140 GHz high-gain LTCC-integrated transmit-array antenna using a wideband SIW aperture-coupling phase delay structure," in *IEEE Trans. Antennas Propag.*, vol. 66, no. 1, pp. 182-190, Jan. 2018.

[10] K. Medrar et al., "H-band substrate-integrated discrete-lens antenna for high data rate communication systems," in *IEEE Trans. Antennas Propag.*, vol. 69, no. 7, pp. 3677-3688, July 2021.

[11] O. Koutsos, F. Foglia Manzillo, A. Clemente and R. Sauleau, "Analysis, rigorous design, and characterization of a three-layer anisotropic transmitarray at 300 GHz," in *IEEE Trans. Antennas Propag.*, vol. 70, no. 7, pp. 5437-5446, July 2022.

[12] R. Sauleau, D. Thouroude, P. Coquet, and J. P. Daniel, “Theoretical reflection coefficient of metal grid reflectors at a dielectric boundary,” in *J. Infr. Millim. Waves*, vol. 20, no. 2, pp. 325-340, Feb. 1999.